~~Combined Hazard~~Multi-hazard Analysis of Flood and Tsunamis on The Western Mediterranean Coast of Turkey

Cuneyt Yavuz [1,~~2~~], Kutay Yilmaz [~~3~~2], Gorkem Onder [~~4~~3]

[1]Department of Construction Technologies, Technical Sciences Vocational School, Dumlupinar University, 43000, Kutahya, Turkey
[~~2~~]~~Graduate School of Engineering, The University of Tokyo, 113-8654, Tokyo, Japan~~
[~~3~~2]ALTER International Engineering Inc. Co., 06800, Ankara, Turkey
[~~4~~3] Sumodel Engineering Inc. Co., 06800, Ankara. Turkey

Correspondence to: Cuneyt Yavuz (cuneyt.yavuz@dpu.edu.tr)

Abstract. Flood has always been a devastating hazard for social and economic assets and activities. Especially, low-land areas such as coastal regions can be more vulnerable to inundations. The combination of different natural hazards observed at the same time is definitely worsening the situation in the affected regions. The goal of this study is to conduct a distinctive ~~combined hazards~~Multi-hazard analysis considering flood hazards with the contribution of potential earthquake-triggered tsunamis that might be observed through Fethiye coastline and city center. For this purpose, tsunami hazard curves are generated based on Monte Carlo Simulations. Comprehensive stochastic hazard analyses are performed considering the aleatory variability of earthquake-triggered tsunamis and epistemic uncertainty of ~~flood~~floods having 10~~-~~, 50, and 100-year return ~~period~~periods. Numerical simulations are conducted to combine the potential tsunamis and flood events that are able to adversely affect the selected region. The results of this study show that the blockage of stream outlets due to tsunami waves drastically increases the inundated areas and worsens the condition for the selected region.

Keywords: Stochastic analysis; Monte Carlo simulation; tsunami simulation; flood; ~~potential combined~~ multi-hazard assessment

1 Introduction

Flood hazards have been one of the most destructive and frequent global-wide natural hazards resulting in loss of lives, livestock, and economic assets (Slater&Villarini, 2016; Alfieri et al., 2017; Kreibich et al., 2017; Qiang, 2019; Zhai et al., 2020). Even though low-land and plain areas where 80% of the world population live can create an easy way for urbanization, they also vulnerable to flood risk and the hazardous effects of floods will increase in the future due to the changing hydrological cycle in recent years (Lamond et al., 2011). As the number of flood hazards increases, the amounts of flood losses are going to follow a parallel trend, accordingly. Hemmati et al. (2020), stated that both the number of floods and destructive economic results have been drastically increased since the 1990s ~~(see Figure 1).~~. Munich RE (2020) has set a natural catastrophe loss

Commented [CY1]: The author completed his research project at UTokyo and turned back to his original department

Formatted: English (United Kingdom)

database on natural disasters since 1980s for analyzing and assessing losses resulted by natural disasters. The database revealed that number of floods and their destructive economic results have an upward trend at global scale.

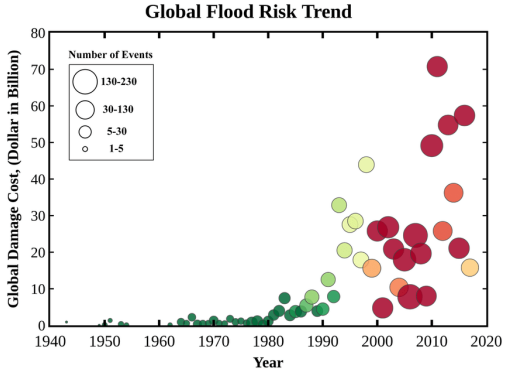

Figure 1. Number of floods and destructive economic results at global scale (Munich Re, 2020)

Independent from flood hazard, the tsunami which can be a long or short-term event is rare but can cause catastrophic damage to economic and social assets and activities (Wolfgang, 2005; Kundzewicz et al., 2017; Subyani et al., 2017; Fukao, 1979). Devastating economic losses and loss of lives have been recorded for the countries that experienced tsunami events, especially for the last two decades (Nadim&Glade, 2006; Carreño et al., 2007; Cardona et al., 2010; Sørensen et al., 2012; Lane et al., 2013; Horspool et al., 2014; Goda&Abilova, 2016). Scientists have revealed significant and reliable hazard evaluation methods for tsunami hazard assessment according to adverse consequences of the experienced tsunamis (Jelínek et al., 2012).

Combined Multi-hazard assessment of floods with different natural hazards can be found in the literature. For instance, climate change-related flood hazard assessment has been widely investigated (Blöschl et al., 2017; Kaspersen et al., 2017; Szewrański et al., 2018; Carter et al., 2018; Barkey et al., 2019). However, the investigations covering simultaneous assessment of flood and tsunami events have been limited. Even if the coincidence of flood and tsunami hazards may be experienced once in a blue moon, it should also be investigated due to the uncertainty of the time of occurrence for these natural hazards. The objective of this study is to reveal a statistical methodology to evaluate the aggregate potential hazard levels due to flood hazards with the presence of earthquake-triggered tsunamis.

As commonly used issues in stochastic hazard analysis of any kind of hazard in the literature (Bommer, 2003; Helton et al., 2010), aleatory and epistemic uncertainties are considered to generate combined multi-hazard analysis in this study. The exceedance of flood hazard is strongly likely depending on geological and meteorological circumstances, the hazard is included in the stochastic analyses conducted in this study as aleatory variability.epistemic uncertainty. Since the occurrence of the tsunami is generally rare compared with flood hazards, tsunami events are inspected by considering epistemic uncertaintyaleatory variability in this study. Additionally, hypothetical earthquake magnitudes M_w are generated using Monte Carlo simulations to obtain a required number of random earthquake sources in the bathymetry.

The proposed methodology is applied to Fethiye city center which is one of the most popular touristic destinations on the Western Mediterranean coast of Turkey. The selection of this site is based on the documented 7 tsunami events throughout the history and evidences of tsunami deposits found by the researchers (Cita&Rimoldi, 1997; Papadopoulos, 2009; Altinok et al., 2011) around Fethiye Bay. Fethiye coastline was hit several times with destructive tsunami waves reaching up to 1.8 m and significant inundation distances were recorded (Papadopoulos, 2009). Location of the study area for the case study is shown in Figure ~~2~~1.

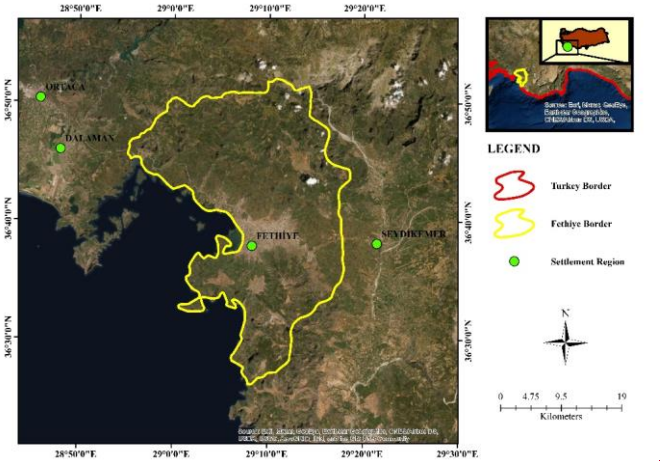

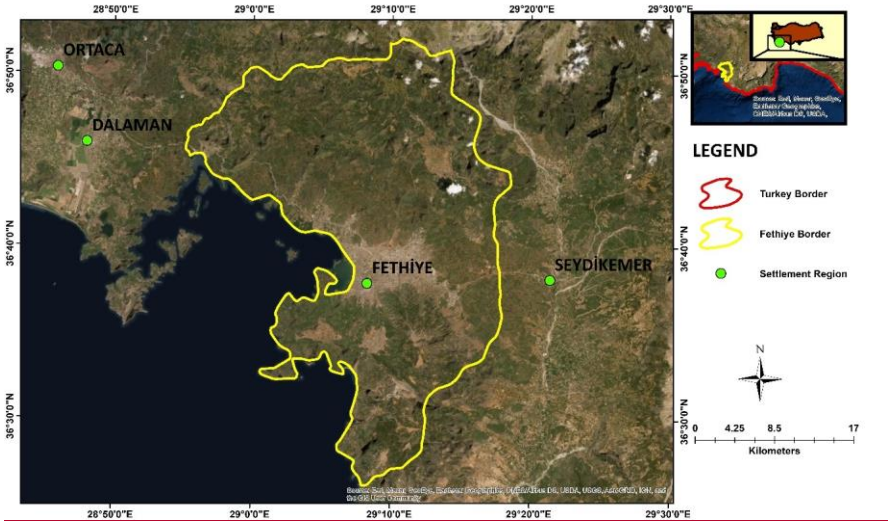

Figure ~~2.~~**1.** Study area and its location on satellite image (Source: Esri, Maxar, GeoEye, Earthstar Geographics, CNES/Airbus DS, USDA, USGS, AeroGRID, IGN, and the GIS User Community~~)~~).

2 Materials and Methods

Probabilistic ~~combined~~ multi-hazard assessment approach ~~(PCHA)~~ is applied in this study. By doing so, the two dynamic natural hazards are aimed to evaluate one by one and simultaneously. 523 historical earthquakes recorded between 1900-2013 are retrieved from European Union funded Tsunami risk and strategies for the European region (TRANSFER, n.d.) project catalogue. Gutenberg-Richter relationship is used to determine the best-fitted distribution for the historical earthquake magnitudes. The Gutenberg-Richter relationship is a mathematical expression of the relationship between a number of earthquakes and the Richter magnitudes (M_w) of these earthquakes that occurred in a specific region (Gutenberg & Richter, 1956). They proposed a widely accepted and commonly used empirical equation that explains the relationship between the occurrence probability of an earthquake depending on two seismic constants (i.e. a and b values) which define the frequency-magnitude distribution and the Richter magnitudes experienced in a particular region. The equation is defined as follows:

$$\log N = -\mathrm{b}M_w + \mathrm{a} \quad (1)$$

where N is the number of earthquakes experienced in the selected region, a and b are the constant that defined specifically for the selected region.

Tsunami hazard curves are generated based on the hypothetical earthquake magnitudes (M_w) produced from 100000 Monte Carlo simulations. Nami-Dance software is used to simulate the hypothetical earthquakes having the $M_w \geq 6.5$ (USGS, n.d.) and resulting in tsunami wave heights are computed at the coast of Fethiye city center.

Flood ~~hazard~~hazards having the recurrence period of 10, 50, and 100 years (Q_{10}~~),~~, Q_{50}, *and* Q_{100}) on the other hand, is modeled by MIKE 11, MIKE 21 FM and MIKE Flood considering with and without tsunami wave existence at the coasts (DHI, 2016). As a more frequent flood period, Q_{10} is evaluated in ~~this study instead of~~detail and hazard maps are generated for the flood events having the return period of 50 years ~~or~~(Q_{50}) and 100 years (Q_{100},) respectively. Additionally, tsunami-drifted flood hazard levels are also provided for all three flood events to satisfy the multi hazard assessment procedure presented in this study. Thus, hazard levels considering both flood, earthquake-triggered tsunami, and tsunami-drifted flood hazards can be compared for the selected region. The inundation levels presented in this study have just resulted from the numerical analysis of both hazards. Potential hazard that can be resulted due to seismicity are not in the scope of this study. The flowchart of the methodology used in this study is illustrated in Figure ~~3~~2.

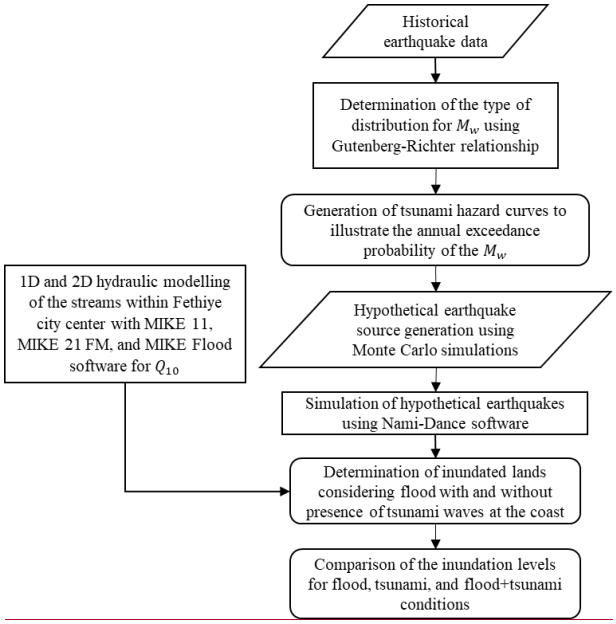

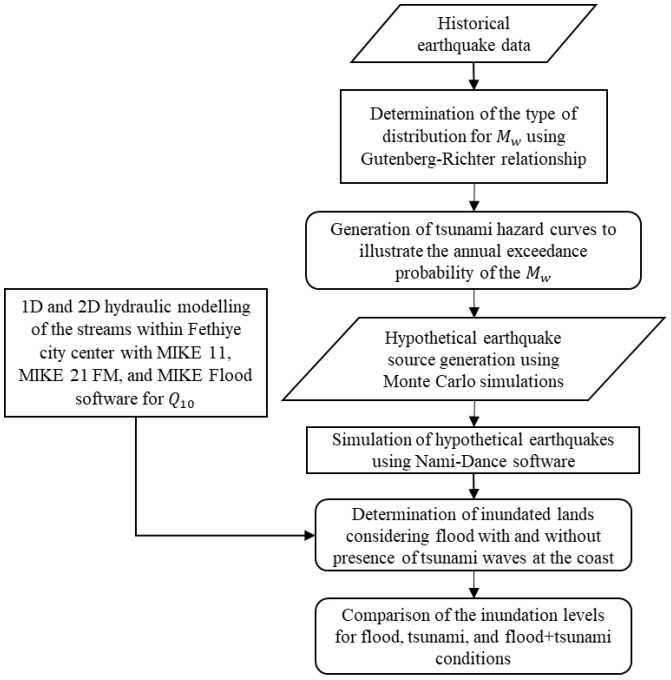

Figure ~~3. Combined~~ 2. Multi-hazard assessment framework used in this study

2.1. Generation of Hypothetical Earthquakes

Random M_w are generated using Monte Carlo simulation, also known as stochastic modeling is accepted as one of the most flexible and easiest methods to implement probabilistic hazard analysis (Ferson, 1996). Probability density function is defined for M_w that defined as the independent parameter of the earthquake. Normal distribution is assigned to M_w depending on the probability density function. Kolmogorov-Smirnov test is applied to the assigned distribution to test the goodness of fit via p-value. Feasibility of M_w data production is satisfied by conducting 100000 Monte Carlo simulations. Sufficiency of the generated data and the consistency of normal distribution are inspected using Gutenberg-Richter Relationship. For Fethiye bay, the a and b values used in the Gutenberg-Richter relationship are obtained from ~~Pamukcu~~Pamukçu et al., (2021) as 4.6624 and 0.8644, respectively. QQ plot obtained from Gutenberg-Richter relationship for the study area is illustrated in Figure ~~4~~3. For the moment magnitudes greater than 6.0 illustrated in Figure ~~4~~3, the normal distribution has a good coincidence with the Gutenberg-Richter relation.

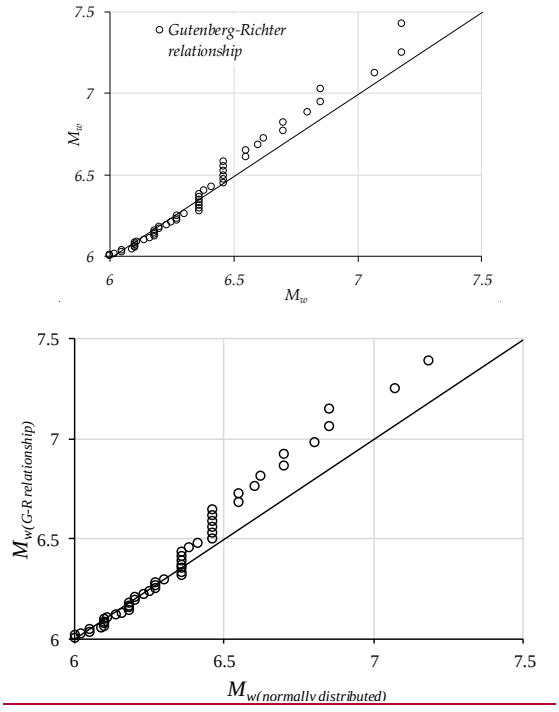

Figure ~~4.~~3. QQ plot of M_w for Gutenberg-Richter law and the normal distribution.

~~Tsunami~~Three different tsunami hazards ~~curves are~~ curve samples that derived from 100000 Monte Carlo simulations are used to determine the reliability of Monte Carlo simulations by considering the ~~epistemic uncertainty~~aleatory variability of each hypothetical earthquake magnitude by checking the consistency of the curves ~~(see~~. The curve samples are shown as Sample_1, Sample_2 and Sample_3 in Figure ~~5).~~4.

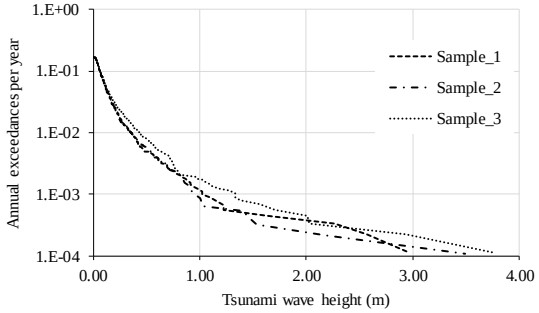

Figure ~~5.~~4. Tsunami hazard ~~curves~~curve samples derived from 100000 Monte Carlo simulations.

Coincidence between the randomly generated M_w shows that 100000 Monte Carlo simulations are sufficient up to 10^{-4}/year annual exceedance of the tsunamigenic earthquake. As clearly stated in the literature, earthquakes having $M_w \geq 6.5$ can be considered tsunamigenic earthquakes (USGS, n.d.). Depending on this statement, 1561 out of 100000 randomly generated M_w has a magnitude greater than 6.5 and is considered tsunamigenic earthquakes in this study. The generation steps of the hypothetical earthquake sources are given in Figure ~~6~~5.

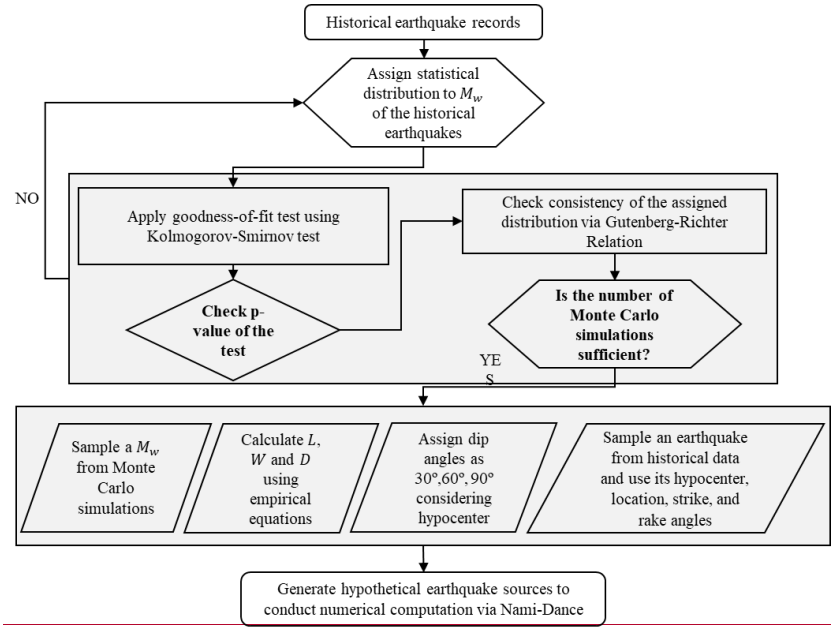

Figure 6. Tsunami hazard curves derived from 100000 Monte Carlo simulations.

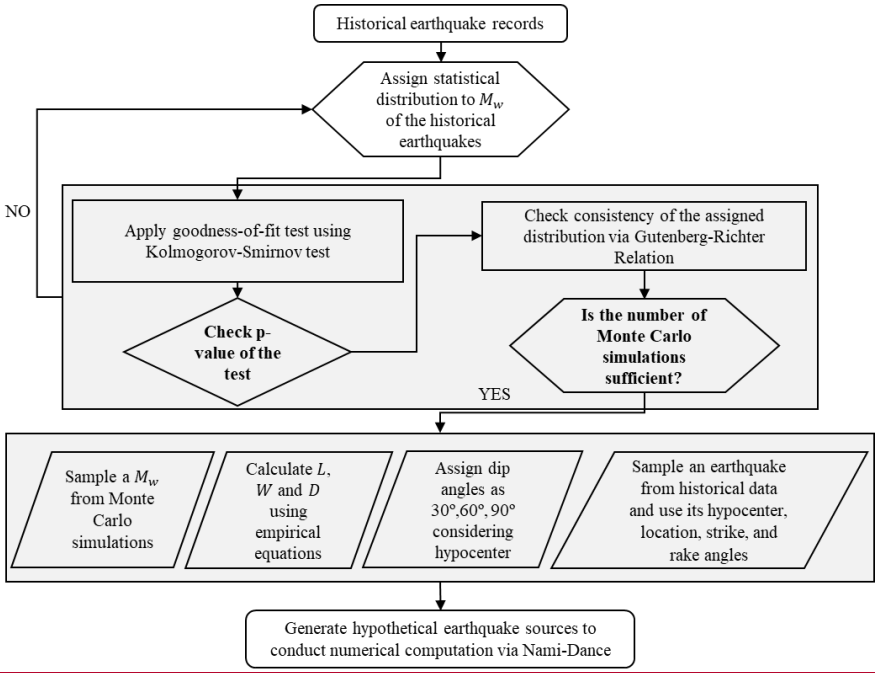

Figure 5. Generation steps of the hypothetical earthquake sources.

The calculation procedure of the parameters of the hypothetical earthquake is explained, respectively. Fault length (L) of the hypothetical earthquake is calculated using the following equation (武村雅之, 1998):

$$logL = 0.5M_w - 1.91 \ \ for\ M_w < 6.8 \quad (1)$$

$$logL = 0.75M_w - 3.77 \ \ for\ M_w \geq 6.8 \quad (2)$$

The fault width (W) can then be calculated using the simple equation given for the rupture area (S) as $W = S/L$. Displacement (D) is also calculated using the empirical equation provided by Hanks&Kanamori, (1979):

$$M_w = {}^{2}/_{3}\, log(M_0) - 10.7 \quad (3)$$

$$M_0 = \mu LWD \quad (4)$$

where μ is the shear modulus of crust ($3.43 * 10^{10}\ N/m^2$).

~~Depending on~~In this study, the asperity position of the hypocenter ~~of the hypothetical~~is assumed to be at the center of the fault and hypocenter distances are directly obtained from the historical earthquake dataset. In some circumstances, hypocenter distances are smaller than the calculated W values. This phenomenon causes some problematic solutions. To prevent this kind

of miscalculations, dip angles are randomly assigned as 30^0,60^0, and 90^0 to the grouped hypocenter distances considering the
130 *W* values as well. The rest of the parameters are obtained directly from a sampled historical earthquake from the catalogue. The locations of the historical earthquakes are randomly assigned as the epicenter of the hypothetical earthquakes and are illustrated in Figure ~~7~~6. Then, these earthquake sources are simulated and tsunami wave heights along the coast of Fethiye, Turkey are computed by Nami-Dance software (Yalciner et al., 2006).

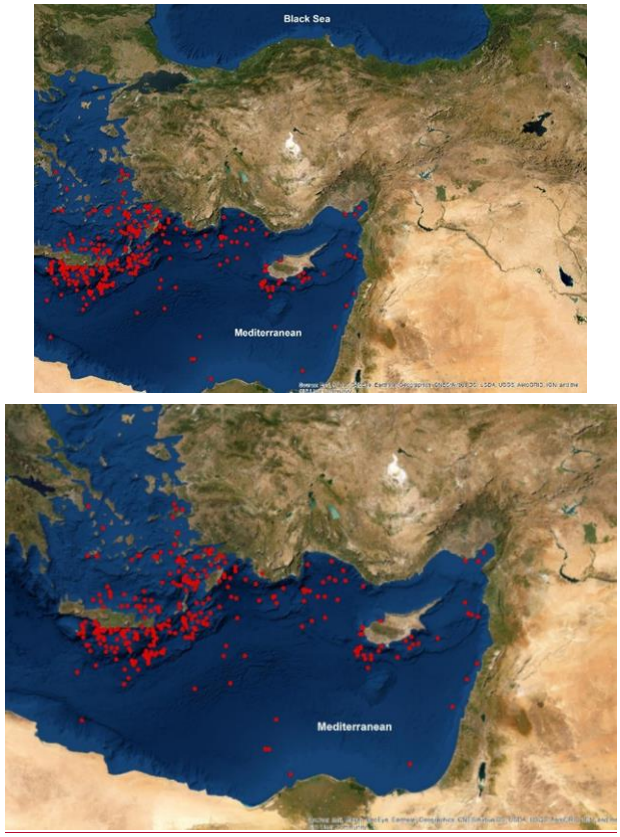

135

Figure ~~7~~6. Historical earthquake locations that used as the epicenter of the hypothetical earthquakes (Source: Esri, Maxar, GeoEye, Earthstar Geographics, CNES/Airbus DS, USDA, USGS, AeroGRID, IGN, and the GIS User Community).

2.2. Tsunami Simulations

100000 earthquake magnitudes are generated via Monte Carlo simulations and 1561 hypothetical earthquake sources having $M_w \geq 6.5$ are compiled to evaluate the flood and tsunami hazards simultaneously for the selected region based on the suggested framework by Yavuz et al., (2020). Bathymetry of the study area has a 407 m grid size is retrieved from the General Bathymetric Chart of the Oceans (GEBCO, n.d.). Nami-Dance software that runs the continuity and momentum equations as shallow water equations is used to perform tsunami simulations to compute the tsunami wave height (d_t) at the coast of Fethiye, Turkey. The shallow water equations are expressed as follows (Velioglu et al., 2016):

$$\frac{\partial \eta}{\partial t} + \frac{\partial M}{\partial x} + \frac{\partial N}{\partial y} = 0 \quad (5\underline{6})$$

$$\frac{\partial M}{\partial t} + \frac{\partial}{\partial x}\left(\frac{M^2}{D}\right) + \frac{\partial}{\partial y}\left(\frac{MN}{D}\right) + gD\frac{\partial \eta}{\partial x} + \frac{gn^2}{D^{7/3}} M\sqrt{M^2 + N^2} = 0 \quad (6\underline{7})$$

$$\frac{\partial N}{\partial t} + \frac{\partial}{\partial x}\left(\frac{MN}{D}\right) + \frac{\partial}{\partial y}\left(\frac{N^2}{D}\right) + gD\frac{\partial \eta}{\partial y} + \frac{gn^2}{D^{7/3}} N\sqrt{M^2 + N^2} = 0 \quad (7\underline{8})$$

$$M = u(h + \eta) = uD \quad (8\underline{9})$$

$$N = v(h + \eta) = vD \quad (9\underline{10})$$

where η is the disturbance at the sea surface due to fault displacement, t is time, x and y are the horizontal axes on the sea surface, n is the Manning's roughness coefficient, M and N are the discharge fluxes, D is the total sea depth, g is the gravitational acceleration, u and v are the water particle velocities and h is the undisturbed sea depth. Nami-dance software has a capability to compute generation, propagation, and amplification of tsunami waves using the shallow water equations given above (Velioglu et al., 2016).

In this study, tsunami wave amplification cannot be calculated due to the coarse grid size of the bathymetry. Therefore, a commonly used empirical equation proposed by Green (Synolakis, 1991; Løvholt et al., 2012,2014; Yavuz et al., 2020) is used to calculate d_t at 1 m water depth at the coast. To apply the equation, a gauge is digitized at 50 m water depth and Green's law (Synolakis, 1991) is used to calculate d_t at 1 m depth at the coast of the selected region.

$$d_t = \sqrt[4]{\frac{h_{50}}{h_1}}\, d_{50} \quad (10\underline{11})$$

where h_{50} and h_1 are the undisturbed water depths at 50 m and 1 m, respectively. d_{50} is the tsunami wave height recorded at the digitized gauge point in the simulation. d_t is used to determine the additional flooded lands resulting from the simultaneous occurrence of the flood and tsunami hazards at the selected regions. The hypothetical earthquakes having the annual exceedance probabilities from 10^{-4}/year to 10^{-1}/year are considered as the earthquakes that can generate a tsunami at the Fethiye coastline. It is known that a tsunami has a wave period of a couple of minutes, while the river flood could be much longer. However, it should be noted here that tsunami hazard assumed to be occurred at the time of fully developed flood hazard condition in this study. By doing so, d_t is considered only as a water level at the downstream boundary condition, it neither

change with time nor the water level at the river mouths. Flood hazard analyses are conducted for the discharge having the recurrence period of 10 years (Q_{10}). Q_{10} flood discharge is selected due to its higher chance of coincidence with a probable tsunami event than other commonly used flood periods in the literature. Thus, the coincidence of the combination of these two hazards changes from 10^{-5}/year to 10^{-2}/year.

2.3. Hydrodynamic Modeling and Quantification of Flood Hazard

~~Flood hazard is~~Fluvial hazards resulting from the water level rise in the river and overflow onto the neighboring lands are also evaluated considering three different return periods with and without the presence of ~~earth-quake~~earthquake-triggered tsunamis. 1D and 2D hydraulic modeling of the streams within the Fethiye City center are conducted by implementing MIKE 11, MIKE 21 FM, and MIKE Flood widely accepted and used software for simulating hydraulic engineering problems (DHI, 2016).

Firstly, 1D numerical modeling is conducted by MIKE 11 which solves Saint Venant's Equations (DHI, 2016). For this purpose, the physical conditions of each stream are determined by field trips. By using the Nivolman GPS device, the layout of cross-sections is determined at every 100 m for each stream. Moreover, the dimensions and locations of culverts or inline structures are determined at the field. Therefore, obtained data from the field are inserted into MIKE 11 to represent the real physical conditions of the study area. Finally, a 1D numerical model via MIKE 11 is conducted and areas prone to flooding are determined by considering the bank elevations and water levels within each cross-section.

After having implemented the 1D numerical model, it is able to conclude that there is a possibility of flooding within the Fethiye City Center. Therefore, MIKE 21 FM model is implemented for the area of the city center. MIKE 21 is widely used software for modeling free-surface flows (DHI, 2016). The software solves shallow water equations which are incompressible Reynolds averaged Navier-Stokes equations (DHI, 2016). Excess discharge within the stream bed (1D model) is released from the river banks and released to the surface thus numerical solution of surface water flows is implemented by MIKE 21. For this purpose, a digital elevation model (DEM) of the area with a resolution of 1 m is obtained from Fethiye Municipality. The DEM of the project area is illustrated in Figure ~~8~~7.

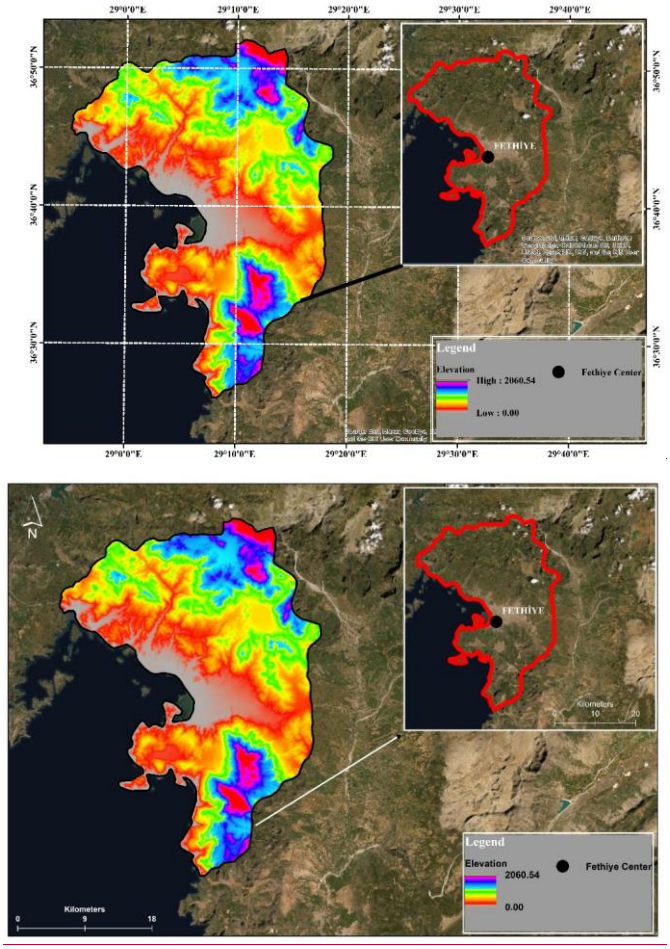

Figure 8.7. Demonstration of the DEM of study area (Source: Esri, Maxar, GeoEye, Earthstar Geographics, CNES/Airbus DS, USDA, USGS, AeroGRID, IGN, and the GIS User Community).

Both the 1D model and 2D model are coupled via MIKE Flood software, thus, excess discharge within the stream bed is released from the banks of the stream and the computational area is inundated. In order to solve the surface flow, the computational domain is meshed with non-uniform unstructured meshes. Moreover, the buildings/structures within the

computational area are digitized and implemented into MIKE 21 model to determine the area with fine meshes. The buildings within the computational area are excluded from the meshing procedure by considering the building elevations and possible inundation water levels. The result is provided by solving 1D and 2D numerical models simultaneously. The stream network of the selected region including Fethiye City Center is presented in Figure ~~9~~8.

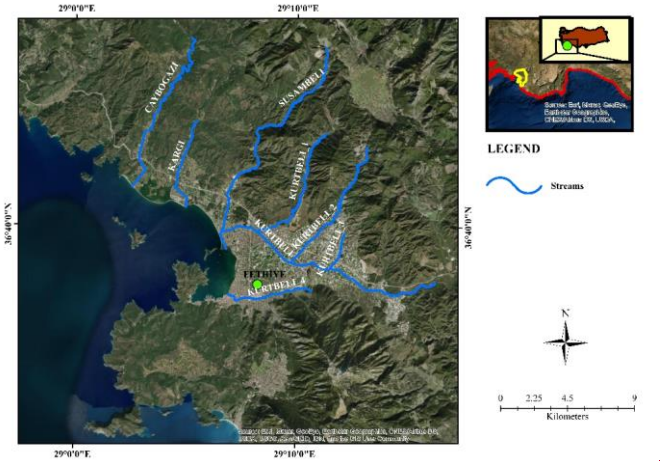

195

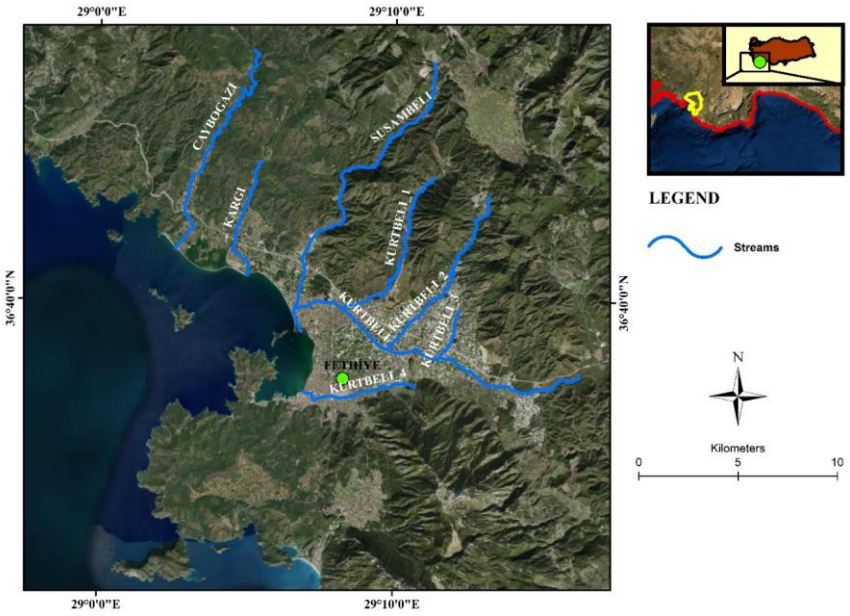

Figure 9.8. Stream network of the selected region (Source: Esri, Maxar, GeoEye, Earthstar Geographics, CNES/Airbus DS, USDA, USGS, AeroGRID, IGN, and the GIS User Community).

Throughout the simulations processes, input boundary conditions of each stream are determined as the discharge of 10 years of recurrence interval (Q_{10}). The calculated Q_{10} discharges for each stream are tabulated in Table 1 and are provided from the "Hydrology Report" of "Flood Management Plan of Western Mediterranean Basin" which was prepared by the General Directorate of Water Management of Turkey under the guidance of "EU Flood Directive 2007/60" and "Water Framework Directive" (SYGM, n.d.).

Table 1. Peak Discharges of the Streams for Discharge of 10 Years Recurrence Interval in the Study Area (SYGM, n.d.).

Fethiye City Center			
Stream	**Q_{10} (m^3/s)**	**Stream**	**Q_{10} (m^3/s)**
Caybogazi	197.88	Kurtbeli_2	11.28
Kargi	32.93	Kurtbeli_3	4.56
Kurtbeli	24.44	Kurtbeli_4	10.16
Kurtbeli_1	19.11	Susambeli	58.2

Formatted Table

Stream	Q_{50} (m³/s)	Stream	Q_{50} (m³/s)
Caybogazi	286.25	Kurtbeli_2	19.02
Kargi	50.95	Kurtbeli_3	5.56
Kurtbeli	45.15	Kurtbeli_4	20.32
Kurtbeli_1	33.46	Susambeli	90.40
Stream	**Q_{100} (m³/s)**	**Stream**	**Q_{100} (m³/s)**
Caybogazi	326.49	Kurtbeli_2	22.58
Kargi	59.38	Kurtbeli_3	10.39
Kurtbeli	55.60	Kurtbeli_4	25.80
Kurtbeli_1	40.53	Susambeli	105.20

The downstream boundary condition for a discharge of having 10, 50 and 100 years return ~~period~~periods of each stream is determined as ~~water~~mean sea level. Moreover, calibration of the hydraulic model is not able to accomplish due to the lack of data. However, the most important parameter for calibrating the hydraulic model is manning's roughness coefficient. The surface roughness coefficients are determined by considering CORINE 2018 Land Cover data (Papaioannou et al., 2018). The computational area was classified according to the land use classification of CORINE 2018 data as shown in Figure ~~10~~9. Spatially varied roughness coefficients of the specific land cover were implemented according to the study conducted by Papaioannou et al., (2018).

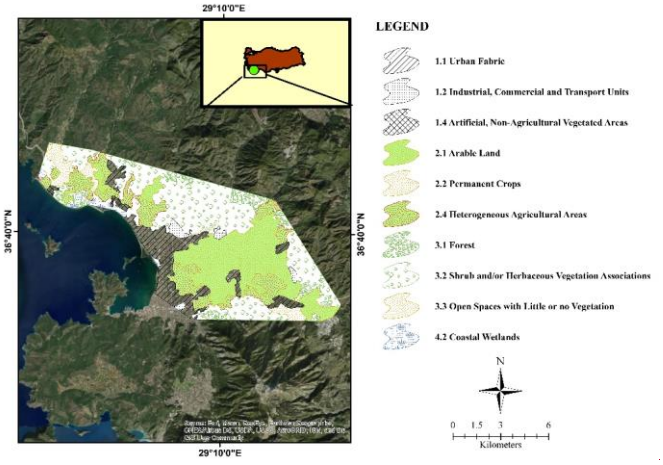

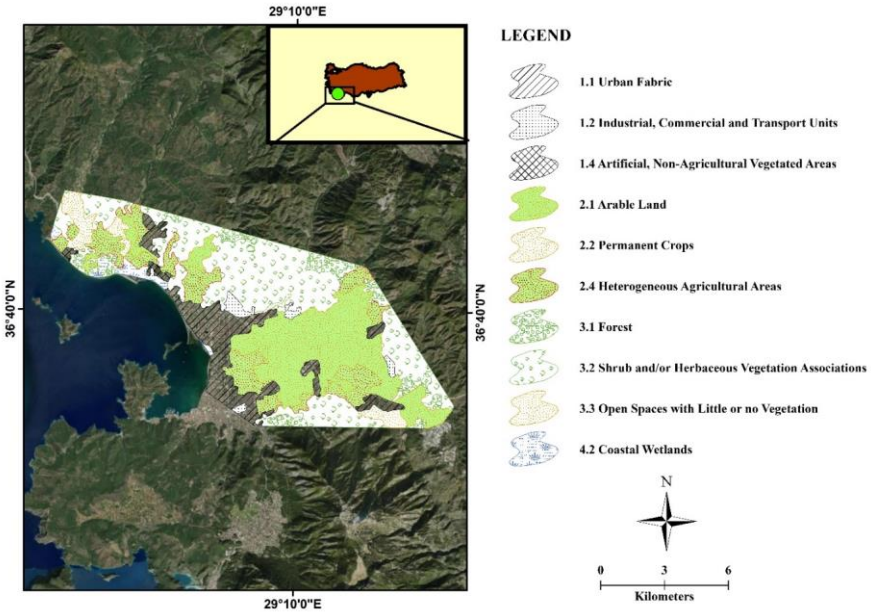

Figure ~~10.~~9. Land cover classification of computational domain according to CORINE 2018 Data (Source: Esri, Maxar, GeoEye, Earthstar Geographics, CNES/Airbus DS, USDA, USGS, AeroGRID, IGN, and the GIS User Community).

Average Manning's surface roughness coefficients study of each land cover of CORINE 2018 data was presented by Papaioannou et al., (2018). The land cover of the computational domain is constructed by examining the CORINE data and the roughness coefficients of each land cover are tabulated in Table 2.

Table 2. Peak Discharges of the Streams for Discharge of 10 Years Recurrence Interval in the Study Area (Papaioannou et al., 2018).

Label 1	Label 2	Manning's n
1 Artificial Surfaces	1.1 Urban Fabric	0.013
	1.2 Industrial, Commercial and Transport Units	0.013
	1.3 Mine, Dump and Construction Sites	0.013
	1.4 Artificial, non-Agricultural Vegetated Areas	0.025
2 Agricultural Areas	2.1 Arable Land	0.~~03~~030
	2.2 Permanent Crops	0.~~08~~080

Formatted Table

Label 1	Label 2	Manning's n
	2.3 Pastures	0.035
	2.4 Heteregenous Agricultural Areas	0.045
3 Forest and Semi Natural Areas	3.1 Forests	0.~~1~~100
	3.2 Scrub and/or herbaceous Vegetation Associations	0.~~04~~040
	3.3 Open Spaces with little or no Vegetation	0..025
4 Wetlands	4.1 Inland Wetlands	0.~~04~~040
	4.2 Coastal Wetlands	0.~~04~~040
5 Water Bodies	5.1 Inland Waters	0.~~05~~050
	5.2 Coastal Waters	0.~~07~~070

Formatted Table

After having carried out the hydraulic analysis, the result of the model is also used for flood hazard quantification. Flood hazard quantification is often conducted by considering water depth and velocity. Although there are various methods for quantifying flood hazards, direct multiplication of depth and velocity is suggested by Smith et al., (2014). The thresholds values for each hazard class and vulnerability classification are tabulated in Table 3 below (Smith et al., 2014).

Formatted: Space Before: 12 pt

Table 3. Hazard Classes and Vulnerability Thresholds (Smith et al., 2014).

Hazard Vulnerability Classification	Description	Classification Limit (m^2/s)
H1	Generally safe for vehicles, people and building	D*V≤ 0.3
H2	Unsafe for small vehicles	D*V≤ 0.6
H3	Unsafe for vehicles, children and the elderly	D*V≤ 0.6
H4	Unsafe for vehicles and people	D*V ≤1.0
H5	Unsafe for vehicles and people. All buildings vulnerable to structural damage.	D*V ≤4.0
H6	Unsafe for vehicles and people. All building vulnerable to failure	D*V ≤4.0

Formatted Table

Water depth within the inundated area and flood propagation velocity are both considered with and without the presence of an earthquake-triggered tsunami. Therefore, spatially varied hazard maps are constructed accordingly.

Formatted: Space Before: 12 pt

3. Results and Discussions

In this study, potential ~~combined~~ multi-hazard assessment because of the fluvial flood hazard (Q_{10}~~)~~, Q_{50}, *and* Q_{100}), with and without the presence of earthquake-triggered tsunamis are analyzed for Fethiye city center. Inundated areas due to flood only,

earthquake-triggered tsunami only, and ~~combined~~ multi-hazard (i.e. flood+earthquake-triggered tsunami) are determined by numerical computations and corresponding inundation levels are revealed for each hazard circumstance.

~~By considering only~~For all flood hazard ~~having 10 years return period~~events considered in this study, maximum water levels are observed within the riverbed. The inundated area due to flood is limited along the streamlines for inland sections. There are also small inundated sections that can be observed due to flood at some parts of the coast of the study area. A large portion of the coastal region is not affected by the flood waves and the inundated area is limited in the coastal parts. ~~A sample~~Sample inundation map of the study area is given in Figure ~~11~~10 for the flood of ~~Q_{10}~~$Q_{10}, Q_{50}, and\ Q_{100}$ obtained from the numerical computations.

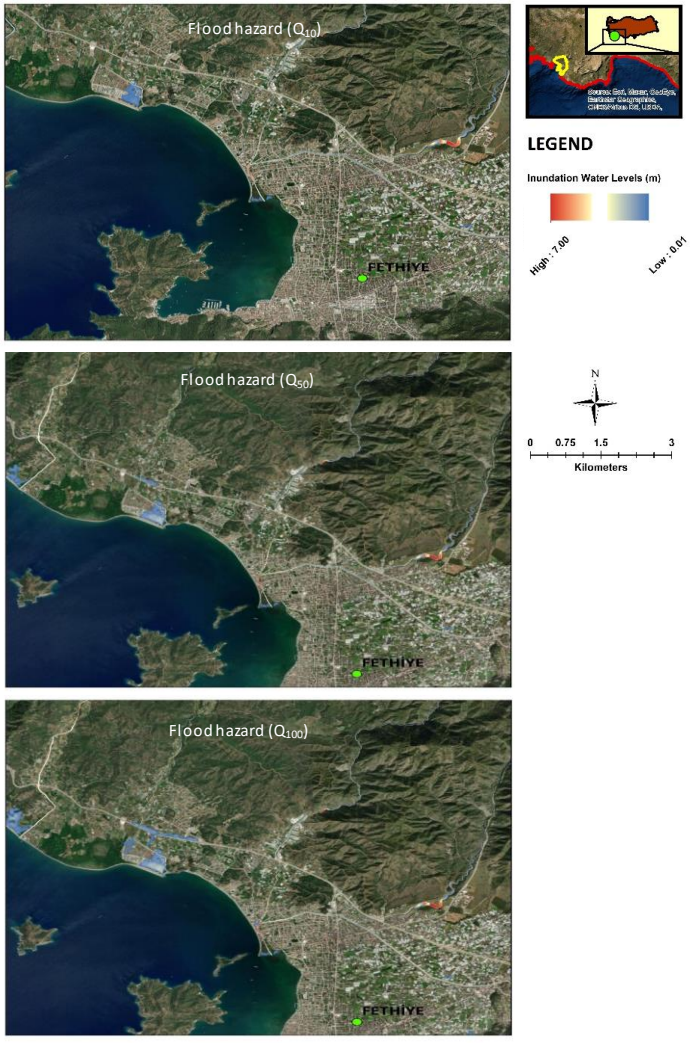

Figure ~~11.~~10. Inundation due to flood ~~hazard.~~hazards considered in the study (Source: Esri, Maxar, GeoEye, Earthstar Geographics, CNES/Airbus DS, USDA, USGS, AeroGRID, IGN, and the GIS User Community).

Although exceeding 6 m water inundation level is observed on some parts of Kurtbeli_1 stream, the effect of Q_{10} flood is limited at the coastline. Depending on the computation results, the other streams also have small inundations around the river beds.

~~For~~ For the flood hazard having 50 years of return period, maximum water levels are observed only within the riverbed again but the inundated area is slightly extended comparing with the flood event having the return period of 10 years as expected. A large portion of the coastal region is not affected by the flood waves and the inundated area is limited in the coastal parts.

Depending on the simulation results, a flood hazard having 100 year return period generates maximum water levels within the riverbeds in the study area. The inundated area due to flood is limited along the streamlines for inland sections. There are also small inundated sections that can be observed due to flood at some parts of the coast of the study area. A large portion of the coastal region is not affected by the flood waves and the inundated area is limited in the coastal parts

For earthquake-triggered tsunami hazard condition on the other hand, significant portion of the coastline estimated to be inundated with 3.5 m tsunami wave heights (see Figure ~~12~~11). Comparing with the flood hazard level, earthquake-triggered tsunamis might have considerable inundation levels at the coastline. Reaching up to 1 km of land from the coastline is estimated to be inundated due to tsunami waves depending on the hypothetical earthquake-triggered tsunami analysis.

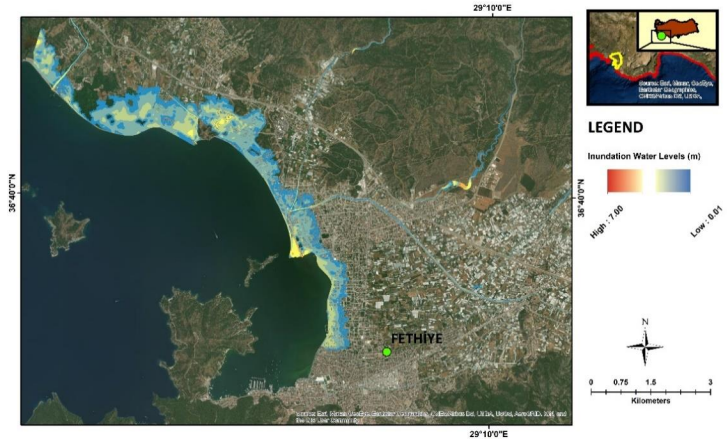

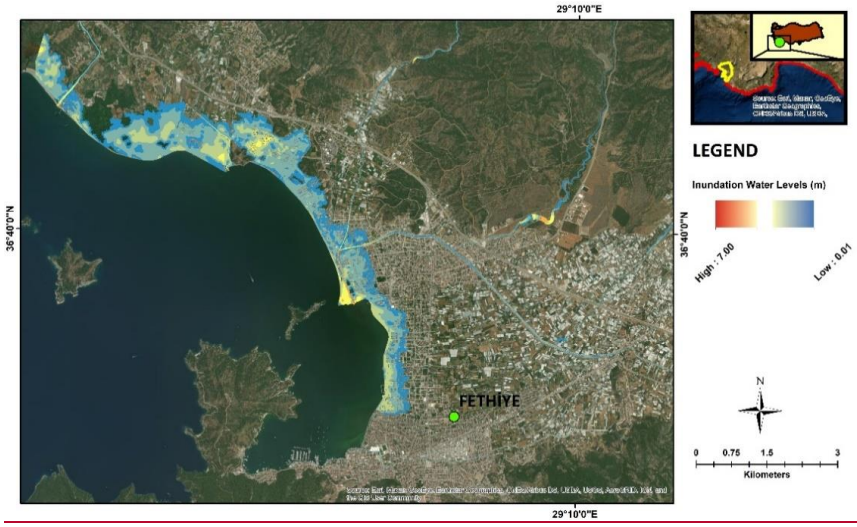

Figure ~~12.~~11. Inundation levels resulted from an earthquake-triggered tsunami hazard (Source: Esri, Maxar, GeoEye, Earthstar Geographics, CNES/Airbus DS, USDA, USGS, AeroGRID, IGN, and the GIS User Community).

On the other hand, the coastline of the study area is severely inundated due to flood (Q_{10}) which was take place slightly before tsunami peak waves hit the coastal parts of the city. Although the maximum tsunami wave height obtained from the simulations is around 3.50 m, the inundation level for the ~~combined~~ multi-hazard existence reaches up to 7.00 m for some parts of the low-lying sections of the study area (see Figure ~~13).~~12).

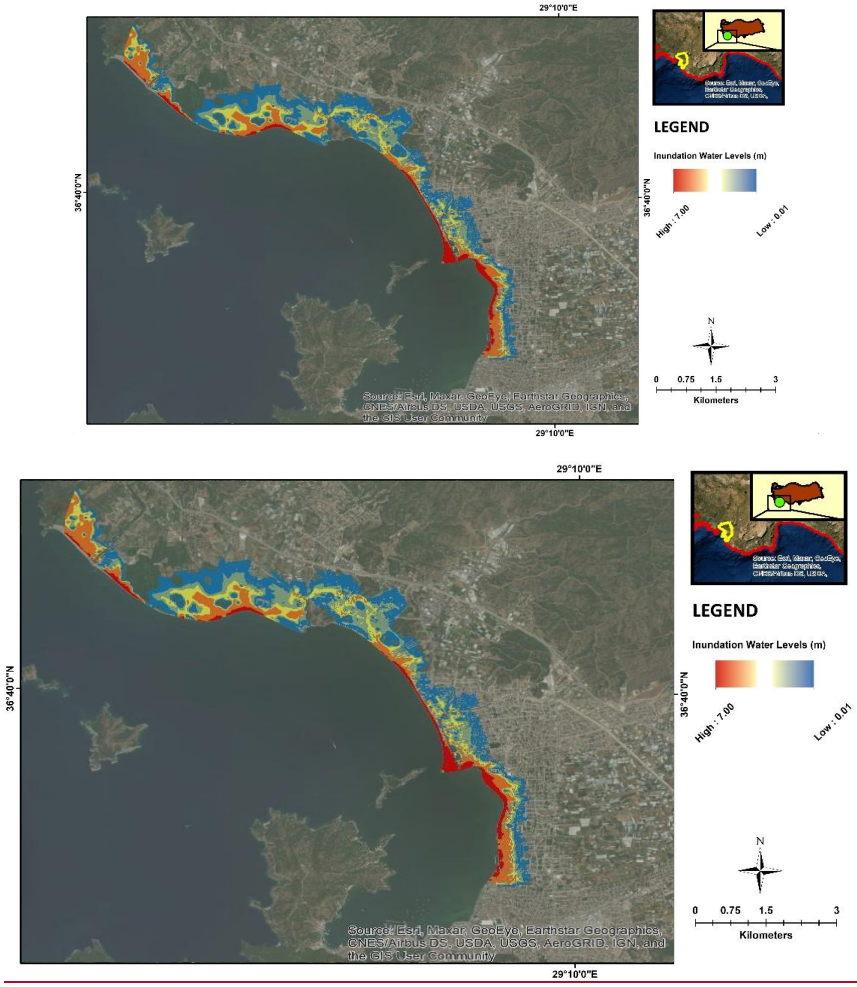

Figure ~~13.~~12. Inundation levels obtained from the simultaneous occurrence of fully developed flood Q_{10} and earthquake-triggered tsunami hazards (Source: Esri, Maxar, GeoEye, Earthstar Geographics, CNES/Airbus DS, USDA, USGS, AeroGRID, IGN, and the GIS User Community).

Even for the contribution of flood hazard having the shortest return period (i.e. Q_{10}) in the study, the multi-hazard inundation level reaches up to 7.00 m. It will not be surprising that higher inundation levels are definitely observed for multi-hazard assessment with Q_{50} and Q_{100} flood hazards.

Quantification of flood hazard is also carried out for all three case studies by considering the threshold values and classes given in Table 3. (Smith et al., 2014). Results of hazard quantification is presented for all return periods in Figure 14~~14~~13.

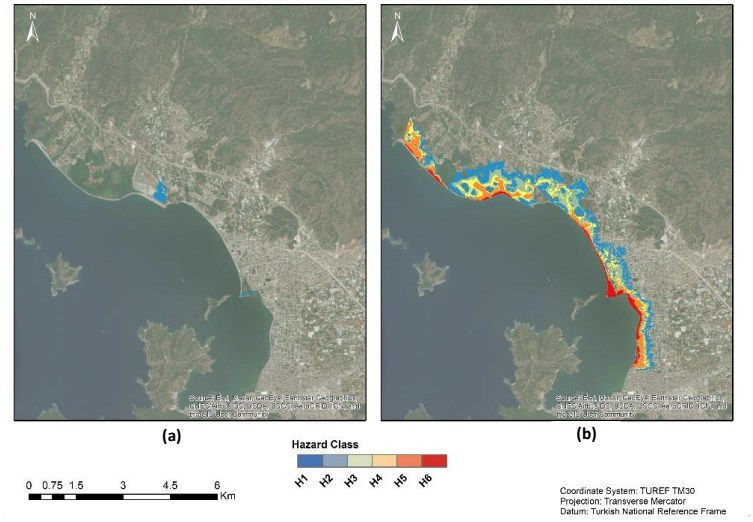

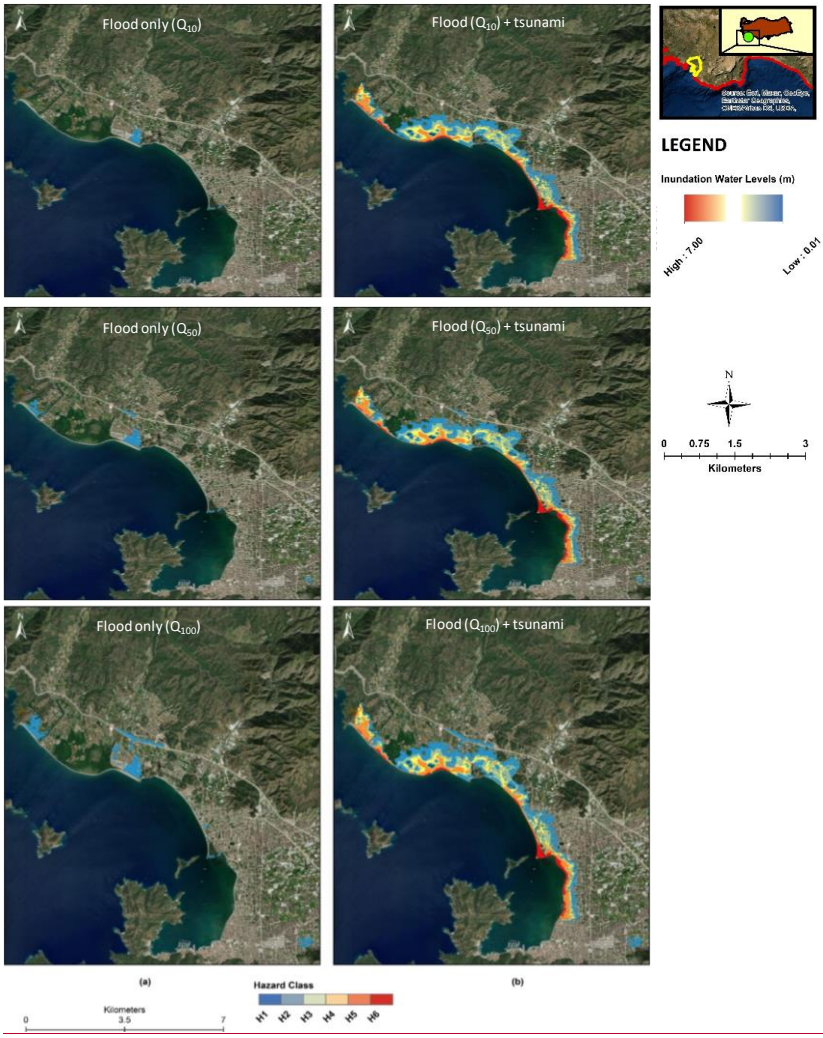

Figure ~~14.~~13. Spatially varied hazard mapping for (a) flood only for Q_{10}, Q_{50}, *and* Q_{100} and (b) multi-hazard condition (i.e. flood+earthquake-triggered tsunami) (Source: Esri, Maxar, GeoEye, Earthstar Geographics, CNES/Airbus DS, USDA, USGS, AeroGRID, IGN, and the GIS User Community).

According to the hazard vulnerability classification proposed by Smith et al., (2014), all three flood ~~of 10 years'~~events having different recurrence ~~interval~~intervals (i.e. 10, 50, and 100 years) drop into H1 hazard class ~~hazard, which~~that can ~~be considered insignificant,~~generate negligible adverse effects in some ~~of the~~ coastal parts of the city center. On the other hand, the fully developed flood ~~of 10 years of~~ events for all three recurrence ~~interval~~intervals just after a peak tsunami waves reach the coast resulted in varying hazard classes of H1 to H6. ~~The~~It should be noted that the major portion of the hazard is caused by the tsunami.

As can be seen from Figure 13 that the inundated area is slightly enhanced due to the rate of change of flood discharges coming from the rivers. However, a huge portion of the hazard is resulted due to the effect of earthquake-triggered tsunamis. It can also be estimated that the rate of change of discharges coming from the rivers may also have some positive effect on the reduction of the additional adverse effect of multi-hazard, due to encountered flows at the coastline.

4. Conclusions

~~Flood~~Fluvial flood hazards having different recurrence intervals and potential earthquake-triggered tsunami hazards are simultaneously analyzed to evaluate the amount of inundation levels at the coastline of Fethiye Bay and Fethiye city center. Results demonstrate that majority of the increase in inundation levels is due to tsunami hazard. However, it should be emphasized that inundation levels are almost doubled in the presence of all flood hazard events at the same time. In the analyses, it is assumed that fully developed fluvial flood take place just after the peak tsunami waves hit the coastal region. Therefore, sea levels are determined accordingly for the hydraulic models.

Flood of 10, 50, and 100 years of recurrence ~~period was~~periods were taken into consideration in the study and potential hazards are calculated. Although it is more sophisticated to reduce the effects of tsunamis, prevention of floods as well as their consequences is a more common procedure. Thus, combined risk analyses of multiple hazards should be taken into consideration in order to reduce risks due to natural disasters.

In conclusion, the coincidence of flood and tsunami events might have a very low chance. But the combination of these two hazards is definitely increased the inundation levels and corresponding disaster levels in the selected region. Some other factors such as seasonal changes in economic and social aspects, the expansion of the residential sites, proximity to the fault zones, and climate change effects should be taken into consideration in combined risk analysis for future years.

Data availability

All raw data can be provided by the corresponding authors upon request.

Author Contributions

CY and KY planned the scope of the study; Methodology prepared by CY; Numerical simulations conducted by CY, KY and GO; Manuscript draft wrote by CY and KY; CY reviewed and edited the manuscript based on the reviewers' comments.

Formatted: Heading 2

Formatted: Normal

Competing interests

The authors declare that they have no conflict of interest.

Acknowledgements

The authors express their appreciation to Prof. Ahmet Cevdet Yalciner and his colleagues to provide Nami-Dance software ver. 9.0 BETA for conducting of tsunami simulations.

Formatted: Normal

References

Alfieri L, Bisselink B, Dottori F, Naumann G, de Roo, A., Salamon P. (2017). Global projections of river flood risk in a warmer world. Earth's Future, 5, 171–182. https://doi.org/10.1002/2016EF000485.

Altinok, Y., Alpar, B., Özer, N., & Aykurt, H. (2011). Revision of the tsunami catalogue affecting Turkish coasts and surrounding regions. Natural Hazards and Earth System Sciences, 11(2), 273-291.

Barkey, R., Nursaputra, M., Mappiase, M. F., Achmad, M., Solle, M., & Dassir, M. (2019). Climate change impacts related flood hazard to communities around Bantimurung Bulusaraung National Park, Indonesia IOP Conf. Ser. Earth Environ. Sci, 235, 1-12.

Blöschl, G., Hall, J., Parajka, J., Perdigão, R. A., Merz, B., Arheimer, B., ... & Čanjevac, I. (2017). Changing climate shifts timing of European floods. Science, 357(6351), 588-590.

Bommer, J. J. (2003). Uncertainty about the uncertainty in seismic hazard analysis. Engineering Geology, 70(1-2), 165-168.

Cardona, O. D., Ordaz, M. G., Marulanda, M. C., Carreño, M. L., & Barbat, A.H. (2010). Disaster risk from a macroeconomic perspective: a metric for fiscal vulnerability evaluation. Disasters, 34(4), 1064-1083, https://doi.org/10.1111/j.1467-7717.2010.01183.x.

Carreño, M.L., Cardona, O. D., & Barbat, A. H. (2007). Urban seismic risk evaluation: a holistic approach. Natural Hazards, 40(1), 137-172.

Carter, J. G., Handley, J., Butlin, T., & Gill, S. (2018). Adapting cities to climate change–exploring the flood risk management role of green infrastructure landscapes. Journal of Environmental Planning and Management, 61(9), 1535-1552.

Cita, M. B., & Rimoldi, B. (1997). Geological and geophysical evidence for a holocene tsunami deposit in the eastern Mediterranean deep-sea record. Journal of Geodynamics, 24(1-4), 293-304.

DHI (2016). Danish Hydraulic Institute- MIKE 11 user guide.

DHI (2016). Danish Hydraulic Institute- MIKE 21 flow model FM Hydrodynamic Module user guide.

Ferson, S. (1996). What Monte Carlo methods cannot do. Human and Ecological Risk Assessment: An International Journal, 2(4), 990-1007.

Fukao, Y. (1979). Tsunami earthquakes and subduction processes near deep-sea trenches. Journal of Geophysical Research, 84(B5), 2303-2314. https://doi.org/10.1029/JB084iB05p02303.

General Bathymetric Chart of the Oceans (GEBCO). Available at: https://www.gebco.net/ (accessed on 04 04 2022).

Goda, K., & Abilova, K. (2016). Tsunami hazard warning and risk prediction based on inaccurate earthquake source parameters. Natural Hazards and Earth System Sciences, 16(2), 577-593.

Hanks, T. C. and H. Kanamori (1979). A moment-magnitude scale, J. Geophys. Res. 84, 2348-2350.

Helton, J. C., Johnson, J. D., Oberkampf, W. L., & Sallaberry, C. J. (2010). Representation of analysis results involving aleatory and epistemic uncertainty. International Journal of General Systems, 39(6), 605-646.

Gutenberg, B., & Richter, C. F. (1954). Seismicity of the Earth 2nd ed., 310 pp. Princeton University Press, Princeton, New Jersey.

Hemmati, M., Ellingwood, B. R., and Mahmoud, H. N. (2020). The role of urban growth in resilience of communities under flood risk. Earth's Future, 8(3), e2019EF001382.

Horspool, N., Pranantyo, I., Griffin, J., Latief, H., Natawidjaja, D. H., Kongko, W., ... & Thio, H. K. (2014). A probabilistic tsunami hazard assessment for Indonesia. Natural Hazards and Earth System Sciences, 14(11): 3105-3122.

Jelínek, R., Krausmann, E., González, M., Álvarez-Gómez, J.A., Birkmann, J., Welle, T. (2012). Approaches for tsunami risk assessment and application to the city of Cádiz, Spain. Natural Hazards, 60, 273-293.

Kaspersen, P. S., Ravn, N. H., Arnbjerg-Nielsen, K., Madsen, H., & Drews, M. (2017). Comparison of the impacts of urban development and climate change on exposing European cities to pluvial flooding. Hydrology and Earth System Sciences, 21(8), 4131-4147.

Kreibich, H., di Baldassarre, G., Vorogushyn, S., Aerts, J. C., Apel, H., Aronica, G. T. (2017). Adaptation to flood risk: Results of international paired flood event studies. Earth's Future, 5, 953–965. https://doi.org/10.1002/2017EF000606.

Kundzewicz, Z. W., Krysanova, V., Dankers, R., Hirabayashi, Y., Kanae, S., Hattermann, F., F., …& Matczak, P. (2017). Differences in flood hazard projections in Europe–their causes and consequences for decision making. Hydrological Sciences Journal, 62(1), 1-14. https://doi.org/10.1080/02626667.2016.1241398.

Lamond, J. E, Booth, C. A., Hammond, F. N., and Proverbs, D. G., (2011). Flood Hazards: Impacts and Responses for the Built Environment. CRC Press – Taylor and Francis Group, London.

Lane, E. M., Gillibrand, P. A., Wang, X., & Power, W. (2013). A probabilistic tsunami hazard study of the Auckland Region, Part II: inundation modelling and hazard assessment. Pure and Applied Geophysics, 170(9-10): 1635-1646.

Løvholt, F., Glimsdal, S., Harbitz, C. B., Zamora, N., Nadim, F., Peduzzi, P., Smebye, H. (2012). Tsunami hazard and exposure on the global scale. Earth-Science Reviews, 110(1-4), 58-73.

Løvholt, F., Glimsdal, S., Harbitz, C. B., Horspool, N., Smebye, H., De Bono, A., Nadim, F. (2014). Global tsunami hazard and exposure due to large co-seismic slip. International journal of disaster risk reduction, 10, 406-418.

Munich Re, (n.d.). https://www.munichre.com/en/solutions/for-industry-clients/natcatservice.html. (accessed on 04 04 2022).

Nadim, F. and Glade, T. (2006). On tsunami risk assessment for the west coast of Thailand. ECI conference on geohazards. Lillehammer, Norway.

Pamukçu, O., Doğru, F., Cirmik, A., & Göneş, D. (2021). Seismic a and b-values and crustal parameters of Samos Island-Aegean Sea, Lesvos Island-Karaburun, Kos Island-Gökova Bay earthquakes. Turkish Journal of Earth Sciences, 30(SI-1), 833-850.

Papadopoulos G. A. (2009). Tsunamis. In: The Physical Geography of Mediterranean, by J.C. Woodward (ed.), Oxford Univ. Press, Oxford, p.493–512.

Papaioannou, G.; Efstratiadis, A.; Vasiliades, L.; Loukas, A.; Papalexiou, S.M.; Koukouvinos, A.; Tsoukalas, I.; Kossieris, P. (2018). An Operational Method for Flood Directive Implementation in Ungauged Urban Areas. Hydrology, 5, 24. https://doi.org/10.3390/hydrology5020024.

Qiang, Y. (2019). Disparities of population exposed to flood hazards in the United States. Journal of environmental management, 232, 295-304.

Slater L J, Villarini G (2016) Recent trends in US flood risk. Geophysical Research Letters. https://doi.org/10.1002/2016GL071199.

Smith, G. P., Davey, E. K., Cox, R. (2014). Water Research Laboratory Technical Report 07: Flood Hazard. University of South Wales, Available at: https://knowledge.aidr.org.au/media/2334/wrl-flood-hazard-techinical-report-september-2014.pdf (accessed on 11 04 2022).

Sørensen, M. B., Spada, M., Babeyko, A., Wiemer, S., & Grünthal, G. (2012). Probabilistic tsunami hazard in the Mediterranean Sea. Journal of Geophysical Research: Solid Earth, 117(B1).

Subyani, D., Daniels, Murray, A., & Kirsch, T.D. (2017). The human impact of floods: a historical review of events 1980–2009 and systematic literature review. PLoS Curr, 5, 1-19.

SYGM, (n.d.), "Taskin Yönetim Planları",Available at: https://www.tarimorman.gov.tr/SYGM/Belgeler/Ta%C5%9Fk%C4%B1n%20Y%C3%B6netim%20Planlar%C4%B1/Bat%C4%B1%20Kardeniz%20Ta%C5%9Fk%C4%B1n%20Y%C3%B6netim%20Planlar%C4%B1.pdf (accessed on 04 04 2022).

Synolakis, C. E. (1991). Green's law and the evolution of solitary waves. Physics of Fluids A: Fluid Dynamics, 3(3), 490-491, doi:10.1063/1.858107.

Szewrański, S., Chruściński, J., Kazak, J., Świąder, M., Tokarczyk-Dorociak, K., & Żmuda, R. (2018). Pluvial Flood Risk Assessment Tool (PFRA) for rainwater management and adaptation to climate change in newly urbanised areas. Water, 10(4), 386.

TRANSFER Project, (n.d.). Available at: https://cordis.europa.eu/project/rcn/81399_en.html. (accessed on 04 04 2022).

USGS, (n.d.). What is it about an earthquake that causes a tsunami? Available at: https://www.usgs.gov/faqs/what-it-about-earthquake-causes-tsunami#:~:text=Magnitudes%20between%207.6%20and%207.8,tsunamis%2C%20especially%20near%20the%20epicenter (accessed on 04 04 2022).

Velioglu, D., Kian, R., Yalciner, A. C., & Zaytsev, A. (2016). Performance assessment of NAMI DANCE in tsunami evolution and currents using a benchmark problem. Journal of Marine Science and Engineering, 4(3), 49.

Wolfgang, K. (2005). Flood Risk = Hazard • Values • Vulnerability. Water International, 30:1, 58-68, DOI: 10.1080/02508060508691837.

Yalciner, A. C.; Pelinovsky, E.; Zaytsev, A.; Kurkin, A.; Ozer, C.; Karakus, H. (2006). Nami Dance Manual. Middle East Technical University, Civil Engineering Department, Ocean Engineering Research Center, Ankara.

Yavuz, C., Kentel, E. & Aral, M. M. (2020). Tsunami risk assessment: economic, environmental and social dimensions. Nat Hazards 104, 1413–1442. https://doi.org/10.1007/s11069-020-04226-y.

Yavuz, C.; Kentel, E.; Aral, M. M. (2020). Climate Change Risk Evaluation of Tsunami Hazards in the Eastern Mediterranean Sea. Water, 12, 2881. https://doi.org/10.3390/w12102881.

Zhai, R., Tao, F., Lall, U., Fu, B. Elliott, J., & Jägermeyr, J. (2020). Larger drought and flood hazards and adverse impacts on population and economic productivity under 2.0 than 1.5 C warming. Earth's Future, 8(7), e2019EF001398.

武村雅之. (1998). 日本列島における地殻内地震のスケーリング則—地震断層の影響および地震被害との関連—. 地震 第 2 輯, 51(2), 211-228. (in Japanese).